Acta Crystallographica Section B
Structural Science
ISSN 0108-7681

Octahedral tilt twinning and compositional modulation in $NaLaMgWO_6$

Graham King,[a]* Susana Garcia-Martin[b] and Patrick M. Woodward[a]

[a]The Department of Chemistry, The Ohio State University, 100 West 18th Ave, Columbus, OH 43210, USA, and [b]Departamento de Química Inorgánica, Facultad de Ciencias Químicas, Universidad Complutense, Madrid 28040, Spain

Correspondence e-mail: gking@chemistry.ohio-state.edu

Received 25 June 2009
Accepted 17 August 2009

A combination of selected-area electron diffraction (SAED), neutron powder diffraction (NPD) and high-resolution transmission electron microscopy (HRTEM) reveals a complex superstructure in the ordered perovskite $NaLaMgWO_6$. Through indexing of SAED patterns the unit-cell dimensions are found to be $46.8 \times 7.8 \times 7.9$ Å, which corresponds to a $12a_p \times 2a_p \times 2a_p$ superstructure of the simple $Pm\bar{3}m$ perovskite unit cell. HRTEM images reveal the formation of an unmistakable stripe contrast that repeats with the same periodicity. Doubling of the *b* and *c* axes is brought about by a combination of layered ordering of Na and La, rock-salt ordering of Mg and W, and octahedral tilting. The *a* axis repeat distance results from a one-dimensional twinning of the octahedral tilts in combination with a compositional modulation. Modeling of the NPD pattern shows that the underlying tilt system is $a^-a^-c^0$ with tilt angles of $\sim 8^\circ$ about the *a* and *b* axes. The octahedral tilt-twin boundaries run perpendicular to the *a* axis and are separated by $6a_p$. Simulated HRTEM images show that octahedral tilt twinning alone cannot explain the stripes seen in the HRTEM images, rather a compositional modulation involving the *A*-site cations is necessary to explain the experimental images.

1. Introduction

The ideal cubic perovskite structure with stoichiometry ABO_3 and space-group symmetry $Pm\bar{3}m$ contains a single formula unit per unit cell. Among ternary oxides it is one of the simplest structure types known, which make perovskites an unlikely topic of study for modern day crystallographers. However, the symmetry can be lowered by a variety of mechanisms, including octahedral tilting (Howard & Stokes, 1998; Woodward, 1997*a*), cation ordering (Lufaso *et al.*, 2006), Jahn–Teller distortions of the octahedra (Carpenter & Howard, 2009*a*,*b*; Lufaso & Woodward, 2004) and ferroelectric-type displacements of the *B*-site cations (Stokes *et al.*, 2002; Aleksandrov & Bartolome, 2001), among others. These distortions complicate the crystallography considerably. The structures that result from various combinations of these symmetry lowering distortions are not only of interest to crystallographers, they often impact the physical properties in a significant way.

There are numerous variants of the perovskite structure which result from the combined effects of octahedral tilting and cation ordering, including rock-salt ordering of the *B*-site cations (Howard *et al.*, 2003), 2:1 and 3:1 ordering of the *B*-site cations (Howard & Stokes, 2004), and layered ordering of the *A*-site cations (Zhang *et al.*, 2006). In unusual cases both *A*-site and *B*-site cations order simultaneously. When this happens the most likely combination is layered ordering of the *A*-site

cations in combination with rock-salt ordering of the *B*-site cations (Knapp & Woodward, 2006; King *et al.*, 2007, 2009). Compared with other perovskites the structures of these doubly ordered $AA'BB'O_6$ perovskites are relatively unexplored.

Although $NaLaMgWO_6$ has been the subject of several studies over the years its true crystal structure appears to be more complex than originally thought. This compound was first reported by Sekiya *et al.* (1984) in the first report of a stoichiometric perovskite that exhibited both layered ordering of the *A*-site cations and rock-salt ordering of the *B*-site cations. The X-ray powder diffraction pattern was indexed using a $2^{1/2}a_p \times 2^{1/2}a_p \times 2a_p$ unit cell (a_p refers to the unit-cell edge of a simple cubic ABO_3 perovskite, ~ 4 Å) and the space group assigned as either $P2_1/m$ or $P2_1$. The structure was later re-investigated by Knapp & Woodward (2006) who carried out a Rietveld refinement of laboratory X-ray powder diffraction (XRPD) data and reported a $2a_p \times 2a_p \times 2a_p$ unit cell with $C2/m$ space-group symmetry.

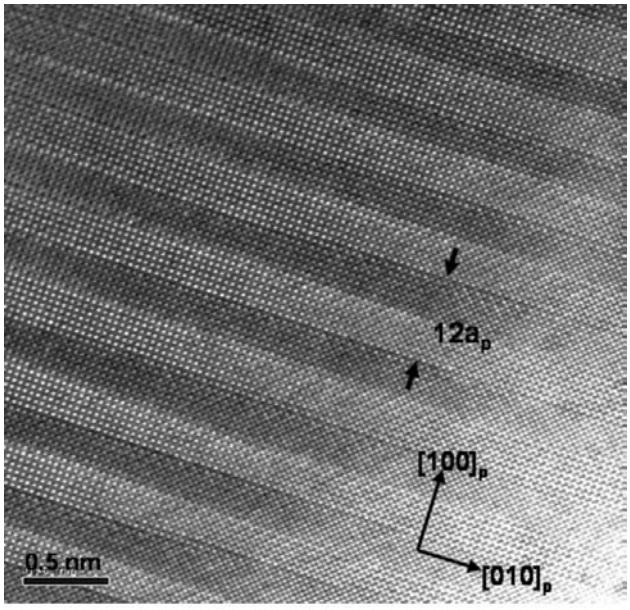

(*a*)

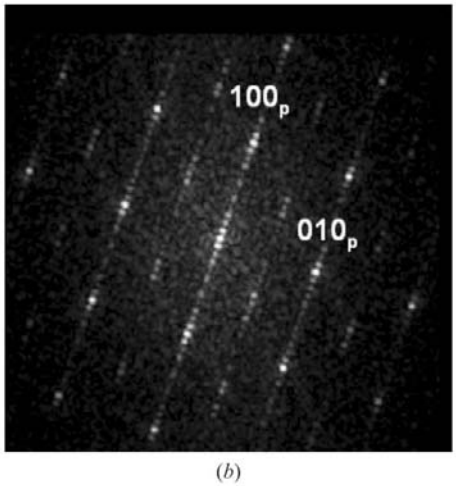

(*b*)

Figure 1
A HRTEM image of a crystal of $NaLaMgWO_6$ along the $[001]_p$ zone axis and the corresponding fast-Fourier transform.

The $C2/m$, $P2_1/m$ and $P2_1$ descriptions can all be realized in doubly ordered $AA'BB'O_6$ perovskites through different patterns of octahedral tilting: $a^0b^-a^0$ ($C2/m$), $a^-a^-c^0$ ($P2_1/m$) and $a^-a^-c^+$ ($P2_1$; Knapp & Woodward, 2006). To resolve controversies surrounding octahedral tilting in perovskites, neutron powder diffraction (NPD) is typically the method of choice. However, subsequent investigation by NPD raised more questions than it answered (Knapp, 2006). The NPD pattern contained satellite reflections that could not be indexed using any space group corresponding to simple in-phase or out-of-phase octahedral tilting. Since satellite reflections were observed in NPD but not in XRPD they were thought to originate from complex effects involving tilting of the octahedra.

A possible origin of this unexpected complexity is periodic twinning of the octahedral tilts. Octahedral tilt twinning in perovskites was first discovered in the *A*-site deficient perovskite $Th_{1/4}NbO_3$ (Alario-Franco *et al.*, 1982; Labeau *et al.*, 1982). In this compound all Th^{4+} ions reside in half-occupied layers which are separated by layers of vacancies. There are two sets of perpendicular twin boundaries each spaced $6a_p$ apart, which run perpendicular to the thorium layers. A similar pattern of twinning was recently used to account for the NPD pattern of another *A*-site deficient perovskite, $(Nd_{7/12}Li_{1/4})TiO_3$ (Guiton *et al.*, 2008). This compound has a similar arrangement of the *A*-site cations and two perpendicular twin boundaries which are spaced $14a_p$ and $28a_p$ apart.

Another possible source of structural complexity comes from the results of a recent transmission electron microscopy (TEM) study of $NaLaMgWO_6$ that revealed an unexpected modulation of the crystal structure (Garcia-Martin *et al.*, 2008). The TEM analysis revealed rather dramatic contrast differences in the high-resolution images. The images show alternating light and dark stripes running perpendicular to the direction of *A*-site cation layered ordering. The stripes are spaced $6a_p$ apart giving a total repeat distance of $12a_p$ (~ 48 Å). Electron energy-loss spectroscopy (EELS) indicated that a compositional modulation of the La^{3+} content occurs with the same periodicity as that deduced by TEM.

With the knowledge of the periodicity of the superstructure gained from TEM we have turned our attention back to the neutron diffraction data in an attempt to explain the satellite reflections and the unexpectedly complex structure of $NaLaMgWO_6$. To account for the NPD pattern of $NaLaMgWO_6$ we have constructed several model structures involving twinning of the octahedral tilt system. We have also used these models to generate simulated TEM images in order to confirm the NPD results and gain information about the compositional modulation.

2. Experimental

The sample was prepared using the ceramic method. Details of the synthesis have been previously reported (Knapp & Woodward, 2006). To obtain high-resolution transmission

electron microscopy images (HRTEM) the samples were ground in *n*-butyl alcohol and ultrasonically dispersed. A few drops of the resulting suspension were deposited in a carbon-coated grid. HRTEM studies were carried out with a JEM 3000F microscope operating at 300 kV (double tilt, 20°; point resolution 1.7 Å). Image calculations were performed using the *Crystalkit* and *MacTempas* programs based on the multi-slice approach.

Neutron powder diffraction (NPD) data were collected at the BT-1 beamline at the NIST Center for Neutron Research. The wavelength of the radiation was 1.5403 (2) Å. The simulated diffraction patterns were generated using the program *Crystal Maker*. The Rietveld refinements were performed using *GSAS* (Larson & Von Dreele, 2004; Toby, 2001).[1]

3. Results

3.1. Transmission electron microscopy

Fig. 1 shows the HRTEM image and the corresponding fast-Fourier transform (FFT) of a region of a $NaLaMgWO_6$ crystal along the $[001]_p$ zone axis. Satellite reflections around the main Bragg reflections characteristic of the perovskite structure indicate a modulation of the crystal structure with a $12a_p$ periodicity. The image shows contrast differences formed by dark fringes intercalated with bright fringes also with a $12a_p$ periodicity. These contrast differences are reproduced in annular dark-field scanning transmission electron microscopy (ADF-STEM) images suggesting a compositional modulation, which is confirmed by STEM-EELS line scans that show a variation of the intensity of the La $M_{4,5}$ edge-signal (Garcia-Martin *et al.*, 2008).

3.2. Construction of model structures

The NPD pattern of $NaLaMgWO_6$ contains a number of satellite reflections that cannot be indexed using any unit cell that results from a combination of layered Na/La ordering, rock-salt Mg/W ordering and simple patterns of octahedral tilting. The most intense satellite reflections are found between 37 and 39° 2θ. Similar satellite reflections are also observed around 61 and 71° 2θ. It is worth noting that these reflections are not observed above the background in the X-ray powder diffraction (XRPD) pattern.

The unit cells that arise when octahedral tilt twinning is taken into account are too large for conventional Rietveld refinement. Therefore, our approach was to generate model structures and compare their simulated NPD patterns with the experimental data. Model structures were derived starting from two basic assumptions:

(i) octahedral tilt twinning is responsible for the satellite reflections seen in the NPD data, and

(ii) the periodicity seen in the electron microscope, $12a_p \times 2a_p \times 2a_p$, is the same as that which gives rise to the satellite reflections in the NPD data.

Taken together these assumptions imply that the octahedral tilt-twin boundaries must be separated by $6a_p$. Model structures were generated in a two-step process. First of all a $2a_p \times 2a_p \times 2a_p$ unit cell with accurate atomic coordinates was generated. The next step was to use this unit cell as a building block to construct an appropriate supercell containing octahedral tilt-twin boundaries.

The starting coordinates used to construct the building blocks were generated using the program *POTATO* (Woodward, 1997*b*). This program generates all of the atomic positions in a $2a_p \times 2a_p \times 2a_p$ perovskite unit cell by assuming tilting of symmetric octahedra. Since the user is allowed to input the magnitude of tilting about each of the three Cartesian axes it is straightforward to generate model structures with different degrees of octahedral tilting. The W—O and Mg—O bond distances were constrained to be 1.917 and 2.100 Å, respectively. These values were calculated from bond-valence parameters using the program *SPuDS* (Lufaso *et al.*, 2006). The Na/La layered ordering was imposed and the *A*-site cations were taken to lie at the same positions they would in a simple cubic perovskite. The *B*-site cations are located at the centers of the octahedra in the unit cells generated by *POTATO*. While this is a fairly reasonable assumption for Mg^{2+} it has been previously established that the smaller d^0 cations (W^{6+} in this case) distort from the centers of their octahedra toward the layer containing the monovalent *A*-site cation (Knapp & Woodward, 2006). In our model structures the W^{6+} ions were displaced by 0.15 Å along the *c* axis towards the Na^+ layer. The magnitude of the displacement was estimated from an analysis of similar known structures (King *et al.*, 2007). The unit-cell dimensions were taken to be equal to the $2a_p \times 2a_p \times 2a_p$ cell reported previously (Knapp & Woodward, 2006).

To construct a $12a_p \times 2a_p \times 2a_p$ supercell one needs to generate the full list of atomic coordinates in a unit cell with *P*1 symmetry. The starting point is the atomic coordinates of the $2a_p \times 2a_p \times 2a_p$ cell described in the preceding paragraph. The origin was shifted from the coordinates given by *POTATO* by $\frac{1}{4}, \frac{1}{4}, \frac{1}{4}$ to simplify later operations. Next, the *a* axis was multiplied by six and the *x* coordinates were divided by six. This generated the first $2a_p$ block (along *a*) of the superstructure. To construct the second and third $2a_p$ blocks of the unit cell the *x*-coordinates of all atoms were shifted by 1/6 and 1/3. At this stage the unit cell is half-filled. The next three $2a_p$ blocks needed to have their tilts twinned relative to the first three. To create these blocks $\frac{1}{2}$ was added to the *x* coordinates of the $2a_p \times 2a_p \times 2a_p$ cell (and then returned to the parent unit cell if $x > 1$) and the *y* coordinates of this cell were inverted. To make the other half of the supercell 1/2, 2/3 and 5/6 were added to these new coordinates. To construct the $12a_p \times 12a_p \times 2a_p$ model the procedure was repeated using the $12a_p \times 2a_p \times 2a_p$ model as the building unit.

The TEM study established that the $12a_p$ periodicity runs perpendicular to the direction normal to the ordered layers of *A*-site cations (the *c* axis). Owing to the pseudo-tetragonal metrics of the underlying subcell, TEM could not distinguish if the *a* or *b* axis was the long axis. For the model structures twin

[1] Supplementary data for this paper are available from the IUCr electronic archives (Reference: HW5005). Services for accessing these data are described at the back of the journal.

boundaries were arbitrarily assigned to run perpendicular to the *a* axis. The cell dimensions of the models with one-dimensional twin boundaries were 46.844 × 7.816 × 7.898 Å with $\alpha = 90$, $\beta = 90.1$, $\gamma = 90^\circ$. Models with these cell dimensions were considered for Glazer tilt systems $a^0b^-a^0$, $a^-b^0b^0$, $a^-a^-c^0$ and $a^-a^-c^+$. The first tilt system, $a^0b^-a^0$, can be immediately discarded because it is not possible to have octahedral tilt-twin boundaries perpendicular to the *a* axis if there is no tilting about the *a* axis. The last tilt system, $a^-a^-c^+$, cannot be realised without severely distorting the octahedra that lie at the boundary. Therefore, this tilt system was also discarded. The final two possibilities $a^-b^0b^0$ and $a^-a^-c^0$ were considered further. They are shown in Figs. 2(*a*) and (*b*).

Studies of octahedral tilt twinning in $Th_{1/4}NbO_3$ (Alario-Franco *et al.*, 1982; Labeau *et al.*, 1982) and $(Nd_{7/12}Li_{1/4})TiO_3$ (Guiton *et al.*, 2008) revealed a two-dimensional network of perpendicular octahedral tilt-twin boundaries. Therefore, despite the absence of two-dimensional contrast in the TEM images, two-dimensional tilt twinning was considered. In order to have a two-dimensional network of twin boundaries there must be tilts about at least two axes. Given the problems already encountered with $a^-a^-c^+$ tilting, it quickly becomes clear that $a^-a^-c^0$ tilting is the tilt system of choice when two-dimensional octahedral tilt twinning is operative. Similar conclusions were reached in earlier studies. This combination could be realised in a model with $12a_p \times 12a_p \times 2a_p$ unit-cell dimensions (Fig. 2*c*).

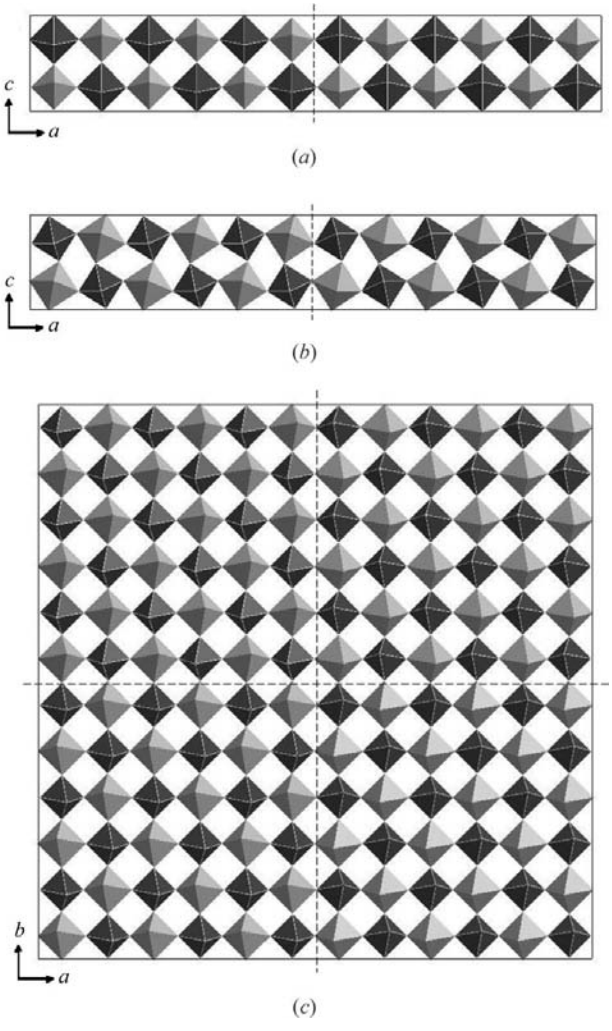

Figure 2
Schemes showing the octahedral tilt twinning for the models constructed for this study. (*a*) A $12a_p \times 2a_p \times 2a_p$ unit cell with $a^-b^0b^0$ tilting and one-dimensional tilt twinning. (*b*) A $12a_p \times 2a_p \times 2a_p$ unit cell with $a^-a^-c^0$ tilting and one-dimensional tilt twinning. (*c*) A $12a_p \times 12a_p \times 2a_p$ unit cell with two-dimensional tilt twinning. Dark grey octahedra are W centered while lighter grey octahedra are Mg centered. The *A*-site cations have been omitted for clarity. Dashed lines show the location of the twin boundaries.

3.3. Neutron powder diffraction

Fig. 3 shows a comparison between the experimental NPD pattern and simulated patterns generated from the various models. The angular range of 36.5 to 39° 2θ is chosen because this is the region of the NPD where the superlattice reflections are most apparent. Fig. 3(*b*) shows the NPD pattern which results from a Rietveld refinement of the structure using the structure of $NaLaMnWO_6$ ($2^{1/2}a_p \times 2^{1/2}a_p \times 2a_p$ cell, $P2_1$ space-group symmetry) as a starting point (King *et al.*, 2007). This model allows for $a^-a^-c^+$ tilting, but does not take into account the possible presence of octahedral tilt twinning. As Fig. 3(*b*) shows, this model generates only two peaks, whereas

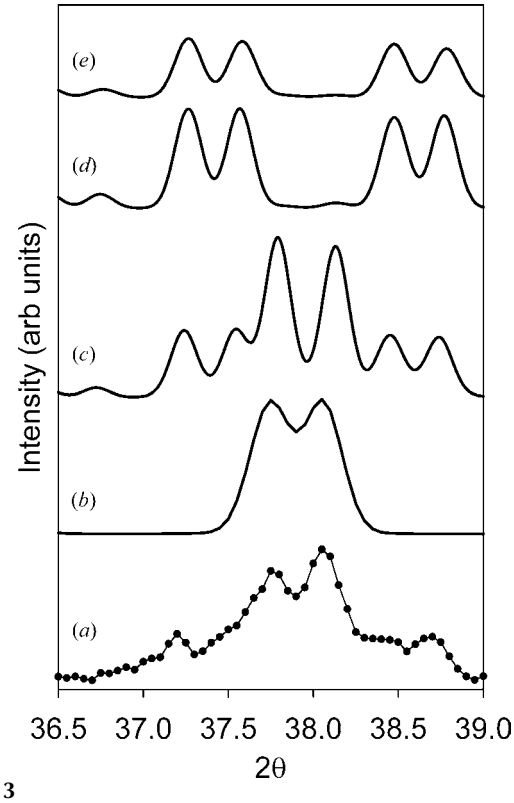

Figure 3
(*a*) The experimental NPD pattern, circles show data points. (*b*) The calculated NPD pattern generated by performing a Rietveld refinement in space group $P2_1$. (*c*) The simulated NPD pattern using $a^-a^-c^0$ octahedral tilting and one-dimensional tilt twinning. (*d*) The simulated NPD pattern using $a^-b^0b^0$ octahedral tilting and one-dimensional tilt twinning. (*e*) The simulated NPD pattern using $a^-a^-c^0$ octahedral tilting and two-dimensional tilt twinning.

the experimental pattern clearly has at least six peaks. Figs. 3(*c*)–(*e*) show the simulated NPD patterns obtained for the model structures shown in Fig. 2. The simulated pattern shown in Fig. 3(*c*) is generated from the model with $a^-a^-c^0$ tilting and one-dimensional octahedral tilt-twin boundaries (Fig. 2*b*). This model generated satellite reflections at the correct 2θ positions with intensities reasonably close to those in the experimental pattern. The simulated pattern shown in Fig. 3(*d*) is generated from the combination of $a^-b^0b^0$ tilting and one-dimensional octahedral tilt-twin boundaries (Fig. 2*a*). This model produced a distinctly different NPD pattern in which the two subcell peaks become nearly extinct and only the satellite reflections are present. This is fundamentally different from what is observed experimentally and therefore this model can be discarded. The simulated pattern shown in Fig. 3(*e*) is generated from the combination of $a^-a^-c^0$ tilting and two-dimensional octahedral tilt-twin boundaries (Fig. 2*c*). It also fails to accurately reproduce the intensities seen in the experimental NPD pattern.

The results shown in Fig. 3 strongly suggest at least part of the structural complexity of $NaLaMgWO_6$ arises from $a^-a^-c^0$ tilting in combination with a periodic one-dimensional twinning of the octahedral tilts. To further assess the validity of this model we considered the agreement with the experimental XRPD pattern. Fig. 4 shows a comparison between the experimental XRPD pattern and a pattern simulated from the same model used in Fig. 3(*c*), focusing on the same region of the diffraction pattern. Note that the satellite reflections are exceedingly weak in the XRPD pattern, which explains why prior studies based on XRPD results did not detect the presence of octahedral tilt twinning (Sekiya *et al.*, 1984; Knapp & Woodward, 2006). Examination of the entire simulated XRPD pattern does not reveal the presence of any substantial supercell peaks.

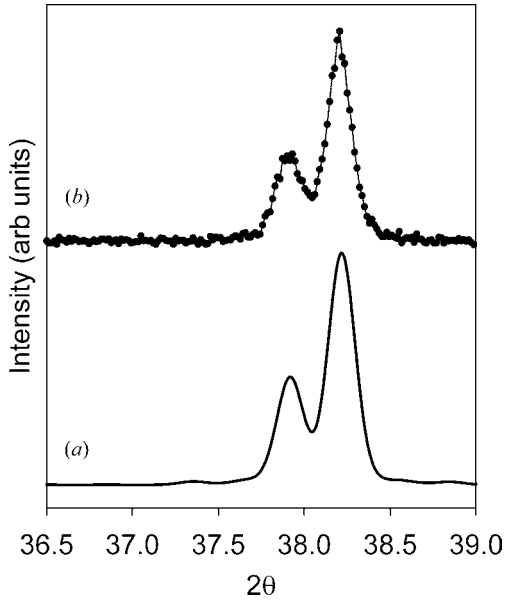

Figure 4
(*a*) The calculated XRD pattern using $a^-a^-c^0$ octahedral tilting and one-dimensional tilt twinning. (*b*) The experimental XRD pattern.

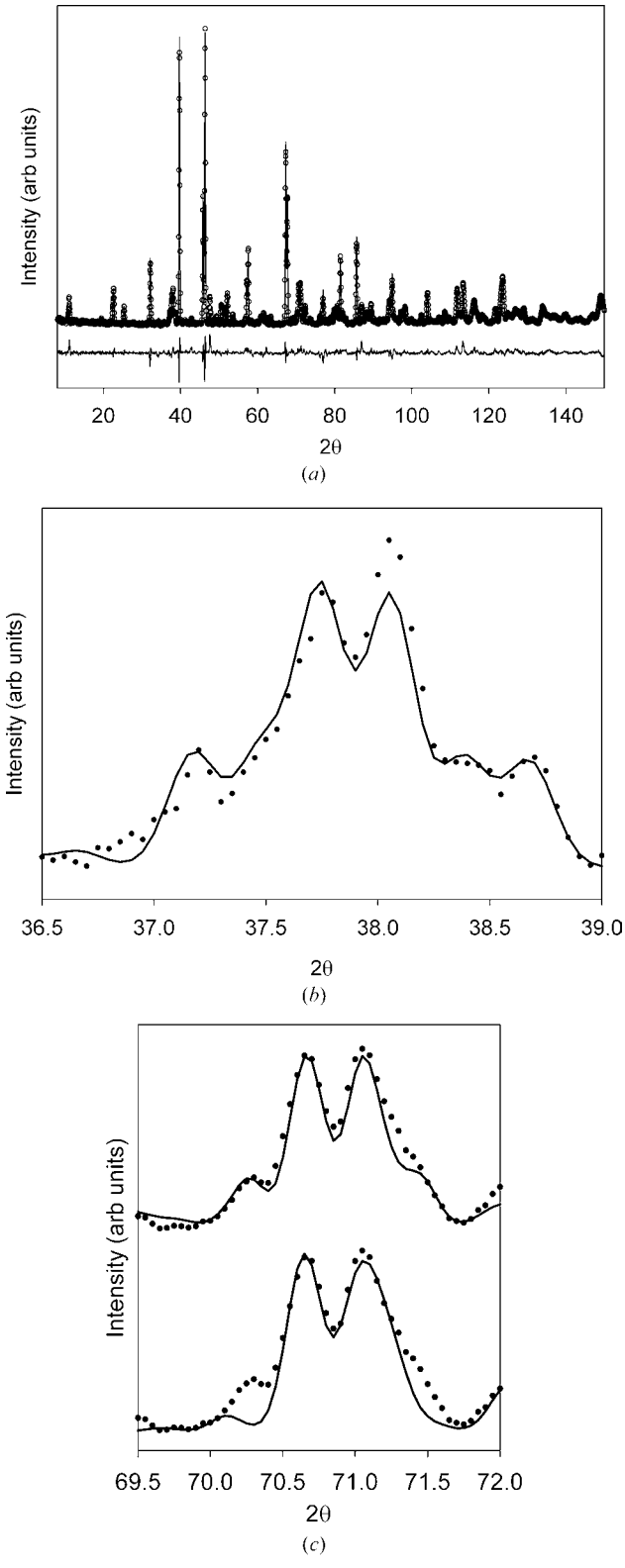

Figure 5
(*a*) The results of the Rietveld refinement using the $a^-a^-c^0$ model and one-dimensional tilt twinning. Open circles are the experimental data points, the solid line is the calculated pattern and the difference is shown beneath. Regions where the satellite reflections are the strongest are shown in (*b*) 36.5–39° and (*c*) 69.5–72.0°. In (*c*) the bottom plot shows the fit obtained using space group $P2_1$ in order to illustrate the improvement upon inclusion of the twin boundaries (top plot).

To validate our model we performed Rietveld refinements using the atomic coordinates of the model structure generated from the combination of $a^-a^-c^0$ tilting and one-dimensional octahedral tilt-twin boundaries. Owing to the very large number of atoms in the unit cell it was not possible to refine atomic positions. The scale factor, background, peak shape, zero point and displacement parameters were allowed to refine. All atoms of the same element were constrained to have the same displacement parameters to reduce the number of variables. The refinement process revealed that the quality of the fit was highly dependent on the tilt angle used to generate the model. In order to properly model the intensities of the satellite reflections the tilt angle needed to be tuned. Refinements were performed using models having tilt angles of 6, 7, 8, 9 and 12° about the *a* and *b* axes. The refinement using an 8° tilt gave the best fit. Attempts to refine occupancies of the *A*-site cations in the hopes of confirming the compositional modulation seen by electron microscopy were inconclusive. Varying the occupancies of the *A* sites did not result in a significant change to the fit.

Despite the fact that no atomic positions were refined, this model was able to produce a reasonable fit to the experimental diffraction pattern. The best fit gave a χ^2 value of 4.00. For comparison, the best fit using the $NaLaMnWO_6$ structure (space group $P2_1$) gave a χ^2 value of 5.01. As can be seen in Fig. 5, the satellite reflections are accurately modeled by this structure. Keep in mind that many of the assumptions used to generate these structures (perfectly rigid octahedra, Mg^{2+} ions lie at the center of an ideal octahedron, the Na^+ and La^{3+} ion positions are fixed) are not constrained by symmetry and therefore only hold in an approximate sense. If the ratio of the number of observations to variables were more favorable (as they would be for a single-crystal sample) and a constrained refinement could be carried out the fit would almost certainly improve significantly. The full crystal structure is shown in Fig. 6.

It should be noted that the twin boundaries do not generate a mirror plane or any other symmetry element in the structure (Fig. 2*b*). In this sense these are not true twin boundaries. Unlike the cases of $Th_{1/4}NbO_3$ and $(Nd_{7/2}Li_{1/4})TiO_3$, the rock-salt ordering of two *B*-site cations in $NaLaMgWO_6$ prevents the generation of a mirror plane at the twin boundaries. The angle of rotation is taken to be twinned, but since the two octahedra that face each other across the twin boundary are of different sizes and have different central atoms, there is no symmetry relationship between them. The space group resulting from $a^-a^-c^0$ tilting in a simple doubly ordered $AA'BB'O_6$ perovskite would be $P2_1/m$. All three symmetry elements of this space group are destroyed by the introduction of the twin boundary. Therefore, the true space group of this compound is $P1$ and all 240 atoms in the unit cell are crystallographically independent. Since the twin boundaries only run in one direction the equivalency of the *a* and *b* axes of tilting is broken and there should be no reason for the tilt angles to be the same. While an $a^-a^-c^0$ model has been used in this study the true tilt system would be $a^-b^-c^0$ with the two tilt angles being nearly, but not exactly, the same. In fact, every oxygen octahedron has a unique environment and may therefore have its own tilt angle and other subtle distortions.

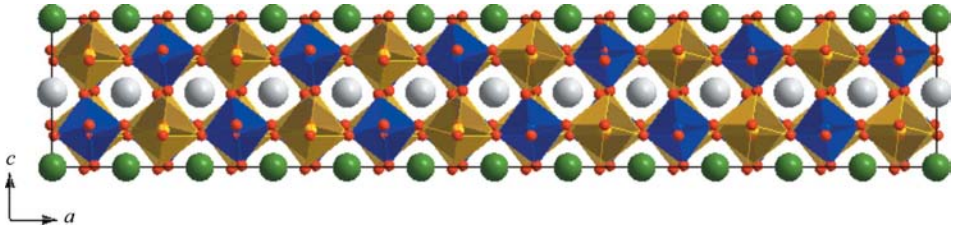

Figure 6
The crystal structure of $NaLaMgWO_6$. One unit cell is shown. The view is looking down the *b* axis. Blue atoms are W, gold atoms are Mg, large grey atoms are Na, large green atoms are La, and small red atoms are oxygen.

4. Discussion

When taken together the NPD and electron microscopy results raise some interesting questions. Can the compositional modulation detected by the ADF-STEM and STEM-EELS measurements be seen in the NPD or XRPD patterns? How much does the octahedral tilt twinning contribute to the stripe contrast seen in HRTEM images? How are the compositional modulation and octahedral tilt twinning related to each other? We consider these questions below.

Simulated XRPD and NPD patterns were created using a model structure that contains both $a^-a^-c^0$ tilting with one-dimensional octahedral tilt-twin boundaries (Fig. 2*b*) and a compositional modulation involving the occupancies of the *A*-site cations. Our previous results confirmed periodic variations of the La content within the domains (Garcia-Martin *et al.*, 2008). We have proposed that the modulation of the La content is most probably due to the replacement of three Na atoms by one La and two vacancies forming alternating stripes with compositions $La(Na_{1-3x}La_x)MgWO_6$ and $NaLaMgWO_6$. Although the exact composition of the Na-deficient domains is not known, as a test the most extreme modulation that maintains charge balance was examined. Namely one where all of the Na^+ sites in one-half of the unit cell are replaced by La^{3+} at 1/3 occupancy to give alternating stripes with compositions of $La_{4/3}MgWO_6$ and $NaLaMgWO_6$, separated by octahedral tilt-twin boundaries.

Simulated XRPD and NPD patterns show that only one additional weak diffraction peak at a *d*-spacing of 46.8 Å ($\sim 1.9°$ 2θ for both XRPD and NPD) is generated by introducing this type of compositional modulation. This falls below the range in which we are able to collect meaningful XRD and NPD data. The peak intensities of the XRD pattern have also proven to be fairly insensitive to the modulation. Since the X-ray scattering power of lanthanum is roughly three times that of sodium this type of substitution has only a very minor effect on

the peak intensities. Unfortunately, the neutron scattering length of La is also roughly three times that of Na. This is why attempts to refine the *A*-site occupancies have not yielded definitive answers. Fortunately, simulations of the TEM images have proven more helpful in this regard.

Different models have been used for the image simulations. The presence of octahedral tilt twinning has been taking into account in all of them. Fig. 7 shows an experimental HRTEM image with several inserts of simulated images. The insert labeled A shows a calculated image (for a 150 Å specimen thickness and a −400 Å defocus of the objective lens) generated by a model which has only a twinning of the octahedral tilt system. Clearly twinning alone does not produce the stripe pattern seen in the experimental image. We also wished to explore the possibility that tilt twinning would impact the displacements of the W^{6+} ions in such a way so as to create stripes in the TEM images. Using bond-valence sums as a guide it can be reasoned that one-dimensional tilt twinning could modify the W^{6+} ion displacements, but only the displacement parallel to the *b* axis. Previous results have shown that the displacement in this direction should be small (King *et al.*, 2007). Based on results from known structures a twinned displacement of 0.07 Å of the W^{6+} ions along the *b* axis was added to the model. The result is simulated image B (for a 190 Å specimen thickness and a −500 Å defocus of the objective lens). This also did not result in a striped pattern.

In order to reproduce the stripe pattern seen in the experimental image it was necessary to vary the composition across the twin boundary. The program used for the simulations does not allow for partial occupancy of sites, therefore approximate compositions were used. Two simulations which have different compositions for the two domains are shown in Fig. 7. The first one (insert C) corresponds to the removal of all the Na atoms and a $\frac{1}{4}$ occupation of the Na layer by La (since small unit cells must be used and fractional occupancies are not allowed it was not possible to use a completely charge-balanced model which corresponded to complete removal of Na). This results in alternation of $NaLaMgWO_6$ and $La_{5/4}MgWO_6$ stripes (for a 120 Å specimen thickness and a −500 Å defocus of the objective lens). The final simulation (insert D) corresponds to a less extreme case where only $\frac{3}{4}$ of the Na are removed and charge compensated by a $\frac{1}{4}$ occupation of this layer by La. This results in a modulation of $NaLaMgWO_6$ and $La_{5/4}Na_{1/4}MgWO_6$ stripes (for a 90 Å specimen thickness and a −600 Å defocus of the objective lens). Both models produce a stripe pattern which closely matches the experimental images, thereby confirming that a compositional modulation is needed to explain the stripe pattern seen in the TEM.

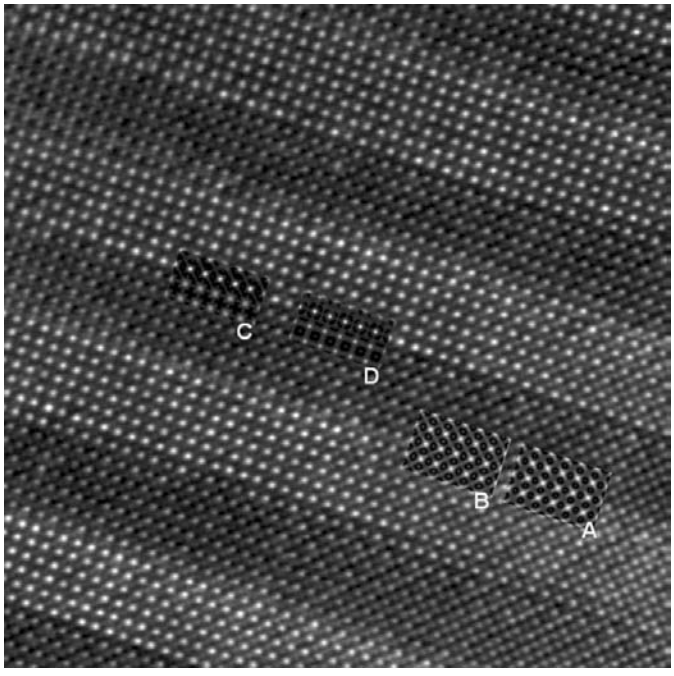

Figure 7
Calculated images inserted into an experimental HRTEM image of a crystal of $NaLaMgWO_6$ along the $[001]_p$ zone axis.

It appears as though octahedral tilt twinning may be fairly common among doubly ordered $AA'BB'O_6$ perovskites. Of the ∼ 30 examples of doubly ordered $AA'BB''O_6$ perovskites that have been reported only nine have been examined by NPD. In three cases, $NaLnMnWO_6$ (Ln = La, Nd, Tb), the NPD data could be accurately refined without resorting to octahedral tilt twinning (King *et al.*, 2007). The NPD patterns of the other six compounds; $NaLaScNbO_6$, $KLaMgWO_6$, $KLaMnWO_6$, $NaNdCoWO_6$ and $NaNdMgWO_6$, all contain satellite reflections not observed in the XRD patterns (King *et al.*, 2007; Knapp, 2006). Preliminary analysis of the neutron patterns of these compounds suggests that the pattern of octahedral tilting and twinning is not the same for all of these compounds. This demonstrates that while octahedral tilt twinning may not be common to all doubly ordered $AA'BB'O_6$ perovskites, neither is it isolated to a few select cases.

The link between compositional modulation and octahedral tilt twinning remains an open question, but some generalities can be made. The prior documented cases of periodic octahedral tilt twinning, $Th_{1/4}NbO_3$ and $(Nd_{7/12}Li_{1/4})TiO_3$, both involve perovskites where a fraction (3/4 and 1/12) of the *A* sites are vacant. In the case of $NaLaMgWO_6$ the working model for describing the compositional modulations involves some degree of substituting an La^{3+} ion and two vacancies for three Na^+ ions, thereby creating a non-negligible concentration of *A*-site vacancies. For example, the overall sample composition used in the TEM image simulation D in Fig. 7 is $Na_{5/8}La_{9/8}\square_{1/4}MgWO_6$. The loss of sodium, and to a lesser extent tungsten and magnesium, may be attributed to the volatility of Na and Mg, or in some cases to the formation of a small amount of Na_2WO_4. It could be that the subtle deviations in composition that enable a compositional modulation are the same ones that stabilize a periodic twinning of the octahedral tilts. It is an undeniable fact that the coordination environment of the *A* sites at the twin boundaries differs from the *A*-site environments found elsewhere in the crystal. Perhaps the larger Na^+ ion is too large for the sites that define the twin boundaries and it is replaced by La^{3+} accompanied by vacancies on either side of the La^{3+} ion. This type of model,

with an overall stoichiometry of $Na_{1/2}La_{7/6}\square_{1/3}MgWO_6$, would be more consistent with the sinusoidal-type modulation of the La^{3+} content seen in the STEM-EELS scans (Garcia-Martin *et al.*, 2008). Other equally plausible models can be hypothesized. At this stage we can only say that further study will be needed to unravel the links between stoichiometry, compositional modulations and octahedral tilt twinning.

5. Conclusions

The combined use of transmission electron microscopy and neutron powder diffraction reveals a strikingly complex structure in the doubly ordered $NaLaMgWO_6$ perovskite. The structure can be described by a triclinic unit cell with dimensions $12a_p \times 2a_p \times 2a_p$. SAED and HRTEM reveal a modulation of the crystal structure with a $12a_p$ periodicity along the $[100]_p$ direction. ADF-STEM images and STEM-EELS scans show that this periodicity involves a repeating pattern of La-rich and La-poor stripes, each $6a_p$ unit cells wide. Analysis of NPD data shows that this compositional modulation is accompanied by a one-dimensional network of octahedral tilt-twin boundaries separated by $6a_p$. The underlying octahedral tilting distortion involves out-of-phase tilts of $\sim 8^\circ$ about the *a* and *b* axes ($a^-a^-c^0$ tilting). The common periodicity suggests that octahedral tilt-twin boundaries and the compositional modulation are related. The results presented here show that NPD patterns simulated from model structures can be used as an effective tool for distinguishing between one-dimensional and two-dimensional networks of octahedral tilt boundaries. It should also be noted that neither the compositional modulations nor the octahedral tilt twinning are apparent from analysis of XRPD data.

P. M. Woodward and G. King thank the NSF for funding through a Materials World Network grant, MWN-0603128, as well as DMR-0907356. S. Garcia-Martin thanks the Spanish MEC for funding Project MAT2007-64486-C07-04 and CAM for Project MATERYENER S 505/PPQ/0358. We acknowledge the support of the National Institute of Standards and Technology, US Department of Commerce, in providing the neutron research facilities used for this work. Thanks to Meghan Knapp and Judith Stalick for collecting the NPD pattern and the Microscopy Centre's Luis Bru from UCM for technical assistance.

References

Alario-Franco, M. A., Grey, I. E., Joubert, J. C., Vincent, H. & Labeau, M. (1982). *Acta Cryst.* A**38**, 177–186.
Aleksandrov, K. S. & Bartolome, J. (2001). *Phase Transitions*, **74**, 255–335.
Carpenter, M. A. & Howard, C. J. (2009*a*). *Acta Cryst.* B**65**, 134–146.
Carpenter, M. A. & Howard, C. J. (2009*b*). *Acta Cryst.* B**65**, 147–159.
Garcia-Martin, S., Urones-Garrote, E., Knapp, M. C., King, G. & Woodward, P. M. (2008). *J. Am. Chem. Soc.* **130**, 15028–15037.
Guiton, B., Wu, H. & Davies, P. K. (2008). *Chem. Mater.* **20**, 2860–2862.
Howard, C. J., Kennedy, B. J. & Woodward, P. M. (2003). *Acta Cryst.* B**59**, 463–471.
Howard, C. J. & Stokes, H. T. (1998). *Acta Cryst.* B**54**, 782–789.
Howard, C. J. & Stokes, H. T. (2004). *Acta Cryst.* B**60**, 674–684.
King, G., Thimmaiah, S., Dwivedi, A. & Woodward, P. M. (2007). *Chem. Mater.* **19**, 6451–6458.
King, G., Wayman, L. M. & Woodward, P. M. (2009). *J. Solid State Chem.* **182**, 1319–1325.
Knapp, M. C. (2006). PhD Thesis, Ohio State University, USA.
Knapp, M. & Woodward, P. M. (2006). *J. Solid State Chem.* **179**, 1076–1085.
Labeau, M., Grey, I. E., Joubert, J. C., Vincent, H. & Alario-Franco, M. A. (1982). *Acta Cryst.* A**38**, 753–761.
Larson, A. C. & Von Dreele, R. B. (2004). *GSAS.* Report LAUR 86–748. Los Alamos National Laboratory, New Mexico, USA.
Lufaso, M. W., Barnes, P. W. & Woodward, P. M. (2006). *Acta Cryst.* B**62**, 397–410.
Lufaso, M. W. & Woodward, P. M. (2004). *Acta Cryst.* B**60**, 10–20.
Sekiya, T., Yamamoto, T. & Torii, Y. (1984). *Bull. Chem. Soc. Jpn*, **57**, 1859–1862.
Stokes, H. T., Kisi, E. H., Hatch, D. M. & Howard, C. J. (2002). *Acta Cryst.* B**58**, 934–938.
Toby, B. H. (2001). *J. Appl. Cryst.* **34**, 210–213.
Woodward, P. M. (1997*a*). *Acta Cryst.* B**53**, 32–43.
Woodward, P. M. (1997*b*). *J. Appl. Cryst.* **30**, 206–207.
Zhang, Z., Howard, C. J., Knight, K. S. & Lumpkin, G. R. (2006). *Acta Cryst.* B**62**, 60–67.